EARTH SURFACE PROCESSES AND LANDFORMS
Earth Surf. Process. Landforms **45**, 224–236 (2020)

Published online 15 November 2019 in Wiley Online Library
(wileyonlinelibrary.com) DOI: 10.1002/esp.4731

Induced biological soil crust controls on wind erodibility and dust (PM10) emissions

Stephen E. Fick,[1,2]* Nichole Barger,[2] John Tatarko[3] and Michael C. Duniway[1]
[1] US Geological Survey Southwest Biological Science Center, Moab, UT USA
[2] Department of Ecology and Evolutionary Biology, University of Colorado, Boulder, CO USA
[3] USDA-ARS Rangeland Resources and Systems Research Unit, Fort Collins, CO USA

Received 17 December 2018; Revised 20 August 2019; Accepted 5 September 2019

*Correspondence to: Stephen E. Fick, US Geological Survey Southwest Biological Science Center, 2290 SW Resource Blvd., Moab, UT 84532 USA. Email: sfick@usgs.gov

ESPL
Earth Surface Processes and Landforms

ABSTRACT: Inducing biological soil crust (biocrust) development is an appealing approach for dust mitigation in drylands due to the resistance biocrusts can provide against erosion. Using a portable device, we evaluated dust emissions from surfaces either inoculated with biocrust, amended with a plant-based soil stabilizer, or both at varying wind friction velocities. Four months after application, emissions from all treatments were either indistinguishable from or greater than controls, despite evidence of biocrust establishment. All treatments had greater surface roughness and showed more evidence of entrapment of windblown sediment than controls, factors which may have been partially responsible for elevated emissions. There was a synergistic effect of inoculation and stabilizer addition, resulting in a nearly two-fold reduction in estimated emissions compared to either treatment alone. Stepwise regression analysis indicated that variables associated with surface crust strength (aggregate stability, penetration resistance) were negatively associated with emissions and variables associated with sediment supply (sand content, loose sediment cover) were positively associated with emissions. With more time to develop, the soil-trapping activity and surface integrity of biocrust inoculum and soil stabilizer mixtures is expected to increase with the accumulation of surface biomass and enhancement of roughness through freeze–thaw cycles. © 2019 John Wiley & Sons, Ltd.

KEYWORDS: PI-SWERL; cyanobacteria; lichen; moss; dust; erosion; aeolian; restoration; Colorado Plateau

Introduction

In the past century, human activity has dramatically accelerated rates of wind-driven erosion and dust emissions in drylands globally (Duniway et al., 2019). Wind-eroded sediment and atmospheric dust are responsible for a broad range of impacts to nature and society (Ravi et al., 2011; UNEP et al., 2016; Middleton, 2017), including soil loss, declines in plant productivity (Okin et al., 2006), damage to property and equipment (Pimentel et al., 1995), disruptions to local and regional hydrology (e.g. via reductions of snow pack; Painter et al., 2007), reductions in visibility causing hazards for human travel (Li et al., 2018), and the genesis of multiple respiratory illnesses (Griffin et al., 2001). Vulnerability to erosion and dust emissions is associated with both geophysical drivers (climate, soils, geomorphology) and anthropogenic disturbance at local and regional scales (Okin et al., 2006; Neff et al., 2008; Reheis and Urban, 2011; Nauman et al., 2018). As both aridity and human activity are likely to increase across drylands (Reynolds et al., 2007; Huang et al., 2016), there is a need for actions to address the drivers and impacts of wind-associated erosion via effective design of monitoring, policy, and restoration techniques (Duniway et al., 2019).

Understanding the controls on dryland erosion processes is critical for developing activities designed to mitigate dust and sediment production. Activities typically involve modifications to the soil surface which either reduce exposure to wind energy, promote surface integrity, or facilitate organisms which perform these functions (Middleton and Kang, 2017). Pits, rocks, perennial vegetation, and other types of barriers and mulches serve to protect soil surfaces and break up connectivity between erosive bare patches (Li et al., 2001, 2006; Okin et al., 2009; Fick et al., 2016), reducing wind energy and trapping the overland flow of sediment (Gonzales et al., 2018). Amendments to the soil surface, such as chemical soil stabilizers strengthen bonds between soil particles, increasing the threshold friction velocity (TFV) at which soil particle movement initiates under shear stress from wind (Armbrust and Lyles, 1975; Yang and Tang, 2012; Zang et al., 2015). Other actions attempt to restore perennial vegetation by direct seeding or addition of soil amendments to improve soil fertility (Monsen et al., 2004; Young et al., 2005; Larney and Angers, 2012). However, many traditional restoration practices, such as large-scale mechanized drill seeding carry significant risk of exacerbating dust production in drylands due to soil disturbance, especially if weather conditions preclude establishment of protective plant cover (Miller et al., 2012; Sankey et al., 2013; Duniway et al., 2015). Designing interventions which minimize risk and cost while conferring long-term stabilization remains a challenge.

One component of dryland systems known to reduce erosion and dust production is biological soil crust (hereafter biocrusts).

Biocrusts are mat-forming consociations of cyanobacteria, lichens, mosses, and fungi which colonize the top 1–2 cm of soil surfaces and bind soil particles together (Belnap and Lange, 2003). Biocrusts have a global distribution, but are most abundant in drylands where competition from plants is reduced, particularly in interspaces (Belnap et al., 2003). Numerous studies have documented erosion-resistant properties of biocrusts (Belnap and Gillette, 1998; Leys and Eldridge, 1998; Hu et al., 2002; Zhang et al., 2006; Thomas and Dougill, 2007; Kidron et al., 2009; Belnap and Büdel, 2016), with some well-developed communities being virtually impervious to wind velocities typically experienced in natural conditions (Belnap et al., 2009). Biocrusts reduce erodibility of surfaces by binding soil particles together through growth of cellular filaments and exudation of extracellular polysaccharides (EPS), shielding surfaces from abrasion (i.e. by sand, microaggregates, and organic matter) with lichen thalli and other cryptogammic structures, and reducing wind energy at the soil surface via generation of surface microtopography (i.e. enhancing effective aerodynamic roughness length; McKenna-Neuman et al., 1996; Hu et al., 2002, Belnap, 2003b). In cold desert locales, surface roughness is particularly pronounced as freeze–thaw cycles may induce pinnacling and undulations in the biocrust soil surface (Belnap, 2003a).

While intact biocrusts are highly resistant to erosion, crushed or trampled biocrusts lose their efficacy and may take years to recover (Belnap, 1993; Belnap and Gillette, 1997). As biocrusts are particularly vulnerable to damage by compressional forces from foot traffic, livestock, or vehicles, extensively disturbed areas may become persistently bare and degraded when coupled with disturbance to vegetation (Miller et al., 2011), and cover significant portions of the landscape (Poitras et al., 2018). Biocrust resistance to disturbance, and subsequent recovery rates tend to be reduced in dry conditions and coarse-textured soils (Belnap and Eldridge, 2003). The observation that many sites remain devoid of biocrusts years after disturbance suggests that some degree of propagule limitation is prohibiting recovery (Bowker, 2007). This has prompted numerous, and largely successful efforts to propagate biocrust inoculum in laboratory and glasshouse settings for potential field inoculations (Mazor et al., 1996; Zhang et al., 2013; Antoninka et al., 2015; Doherty et al., 2015; Velasco Ayuso et al., 2017). However, there are far fewer examples of successful biocrust introductions in the field.

In the field, biocrust recovery may be limited by abiotic stresses (e.g. extremes in temperature or moisture), or poor availability/adaptation of biocrust propagules at a site (Bowker, 2007; Antoninka et al., 2017; Velasco Ayuso et al., 2017). Burial, abrasion and detachment by wind and sand is a common cause of biocrust deterioration in natural settings (Jia et al., 2008; Kidron and Zohar, 2014; Kidron et al., 2017), and may be particularly prevalent in disturbed contexts with unstable soils. Assuming that soil stability may thus be a prerequisite for successful biocrust establishment, the simultaneous addition of biocrust inoculum with artificial soil stabilizing agents may be a promising method for long-term erosion mitigation. This method combines the traditionally effective but short-lasting effects of amendments with longer-term stabilization by biocrusts. Previous studies combining biocrust and stabilizers have found that stabilizing compounds have had neutral (Chandler et al., 2018) to positive effects (Park et al., 2016; Peng et al., 2017; Chock et al., 2019) on biocrust organism development, while also providing short-term stability to soils. Stabilizers may serve to anchor inoculum, provide substrate for micro-organism growth, and reduce overall local fluxes of sand and debris (Lyles et al., 1974; Armbrust and Lyles, 1975; Park et al., 2014).

Induced biocrusts have been shown to be resilient to windshear stress in laboratory settings (McKenna-Neuman et al., 1996; Hu et al., 2002), however little is known about the erosion-mitigating properties of induced biocrust or combinations of biocrust and stabilizers in the field. This lack of information is partly due to the few examples of successful field establishment of induced biocrusts, as well as the use of coarse proxy indicators to assess erodibility (Chiquoine et al., 2016), rather than process-based simulations or measurements. In this study we assess the susceptibility to wind erosion of combinations of rapidly induced biocrusts (over a period of four months) and an organic stabilizer using a portable in-situ wind erosion laboratory (PI-SWERL, Etyemezian et al., 2007), which measures the shear-induced efflux of particles less than the aerodynamic diameter of 10 μm (PM_{10}), an officially recognized air pollutant in the United States (US EPA, 1999). We expected that induced crusts would have reduced emissions relative to control, and that emissions would be further reduced with simultaneous application of soil stabilizer.

Methods

Study site

Experiments were conducted at an abandoned pasture at the Dugout Ranch, part of the Canyonlands Research Center in south-eastern Utah (38.070, -109.564; https://canyonlandsresearchcenter.org/). The ranch is located in the Colorado Plateau physiographic region, composed predominantly of broad, gently sloping valleys surrounded by sandstone outcrops and cliffs. The climate is cool desert, with a mean annual temperature of 15 °C and a mean annual precipitation of 197 mm (Urban, 2017). Approximately 50% of precipitation falls in the cool season (October–May) as frontal storms and 50% falls in the warm season as 'monsoonal' thunderstorms (June–September). Inter-annual variability in precipitation is high, ranging from 124 to 319 mm (CV = 0.25). The average peak wind speed per hour (2 m height) at the site is 2.8 m s^{-1}, with an inter-quantile range between 1.61 and 3.68 m s^{-1}. Average windspeeds are greatest in the spring months (3.6 m s^{-1} average for April). Annual horizontal sediment fluxes at 15 cm above ground level recorded near the site were 1.68 g m^{-2} d^{-1} (615 g m^{-2} total) in 2018, much of which occurred during an intense windstorm ('haboob') in late July (figure 5b in Duniway et al., 2019; US Geological Survey [USGS], unpublished data). Estimated fluxes during the period of this study totaled 0.67 g m^{-2} d^{-1} (80.7 g m^{-2} total; USGS, unpublished data).

Soils at the site belong to the Mivida series (Ustic Haplocalcid), and are attributed to the Semidesert Sandy Loam Fourwing Saltbrush ecological site by the US Department of Agriculture, Natural Resources Conservation Service (035XY215UT; US Department of Agriculture, Natural Resources Conservation Service, 2009). Soils in the top 10 cm of the Mivida series generally have high sand contents (68%), low clay contents (10%) and low amounts of organic matter (~ 1.5%, USDA NRCS, 2009). The site was located in a gently sloping (< 3% grade), west-facing section of the pasture, enclosed by a barbed-wire fence in late 2017 to exclude livestock. The site has been grazed by domestic livestock for over 100 years and has been periodically irrigated through approximately 2003. Past heavy land use has led to severely truncated soils, absence of native perennial vegetation and dominance by invasive annual weeds including *Salsola* sp. and to a lesser extent *Bromus tectorum*. Surfaces exhibited symptoms of highly eroded soils for the region, with patchy deposits of mobile sediment forming temporary coppice 'dunes' around annual plant

skeletons across otherwise bare exposures of finer-textured subsoils. There was no evidence of biocrust development on any surface, likely related to the highly disturbed nature of the site. Based on ecological site description and uncultivated areas nearby, these sites would likely support a mix of biocrusts, C3 and C4 perennial bunch grasses (*Achnatherum hymenoides*, *Plueraphis jamesii*, *Sporobolus* sp.) and shrubs (*Atriplex canescens*, *Sarcobatus vermiculatus*). Due to the absence of biocrusts and native perennial vegetation at the site, as well as the prevalence of bare soil and exotic annuals, it is likely that the site exists in a persistent degraded 'Annualized-Bare' ecological state frequently described for this region (Miller et al., 2011; Duniway et al., 2016; Poitras et al., 2018).

Experimental design

Biocrust for inoculation was collected from two locations within 5 km of the experimental site: (1) a location with well developed, late successional crust containing a rich assemblage of lichen species (Rizno Series, Lithic Ustic Torriorthent; Semidesert Sandy Loam Utah Juniper/Blackbrush: R035XY236UT) and (2) a location characterized by more disturbed, early successional crust with higher moss and light cyanobacteria contents (Redbank Series, Ustic Torrifluvent; Semidesert Sandy Loam Fourwing Saltbrush: 035XY215UT). Biocrust samples were air-dried, crumbled, sieved (rejecting particles < 1 mm), and portioned based on mass/area ratios estimated from stratified samples across inoculum stocks. To calculate mass/area, we divided the mass of biocrust aggregates distributed throughout a petri dish to a depth of 1 cm against the petri dish's areal footprint. Biocrust aggregates ranged in size from 0.2 to 3 cm in diameter, with the majority being approximately 1 cm.

Treatments were applied to 0.5 m^2 plots (0.71 m × 0.71 m) in a factorial combination of three levels of biocrust inoculation (0, 20 and 40% cover, corresponding to 0, 1.5 or 3 kg m^{-2} respectively) crossed with two levels of 'M-Binder' psyllium-based soil stabilizer (Ecology Controls, Carpinteria, CA, USA), either at 0 or 60 g m^{-2}. Treatments were arranged in six blocks of 12 plots for a total of 72 experimental units. Treatments were applied in early February 2018 by distributing pre-weighed mixed inoculum and powdered soil stabilizer evenly across plot surfaces, lightly watering after application.

Six additional plots were identified for later comparisons (hereafter 'reference plots'). Three plots within the boundaries of study site were cleared of vegetation but otherwise untreated (hereafter 'Reference Bare'), and three plots were located in an adjacent area with similar soils but no history of cultivation and moderate levels of natural biocrust development ('Reference Biocrust').

Plots were watered frequently throughout the winter and spring, with breaks between water events not exceeding 1.5 weeks. On watering days, plots were repeatedly sprayed by hand with a low-pressure sprinkler nozzle to the point of surface saturation but not ponding. Water was charcoal filtered prior to application to avoid adverse effects of chlorine on biocrust growth. Dates and volumes of water additions, natural rainfall, and estimated duration of surface wetness are reported in Supporting Information Table S1. In early March, a canopy of 40% transmittance shade cloth was suspended over plots to extend the duration of hydrated conditions suitable for biocrust growth following manual watering and precipitation events (UV Polyethylene Knitted Shade Cloth – 60% Green, DeWitt, Sikeston, MO, USA). Shade cloth was stretched over rebar superstructures fitted with guy-wires, suspended at least 10 cm above plot surfaces, with the outer edges of shade cloths staked to the ground (Figure 1E). The shade cloth was found to be permeable to water added to the plots and larger precipitation events.

Sampling

In early June 2018, immediately prior to each wind erosion simulation, plots were sampled for soil surface characteristics. Soil aggregate stability was assessed from six samples per plot, regularly spaced along the plot's diameter, using a field aggregate stability test kit (Seybold and Herrick, 2001). Surface cover (e.g. soil aggregates, loose erodible material [LEM], soil surface moisture, and physical and biological soil crusts) was assessed using a 0.71 m × 0.71 m pinframe with a grid of 7 × 7 sampling intersections following classes described in Herrick et al. (2005), with modifications used by the National Wind Erosion Research Network (Webb et al., 2016). We did not discriminate between physical crusts and light-pigmented cyanobacterial biocrusts in surveys, since the two cannot reliably be distinguished without disturbing the soil surface. Roughness was assessed by comparing the apparent overhead length of a 54 mm jewelry chain laid flush against the soil surface to its linear length to create a roughness index (Saleh, 1993). The index was calculated as one minus the mean of two perpendicular measurements across each plot. Surface stability was assessed following two methods shown by Li et al. (2010) to be correlated with the threshold friction velocity of the soil surface: (1) measuring the dimensions of impact craters from 4.5 mm diameter copper spheres (BBs) shot from a pumpmaster 760 airgun (Crosman, Bloomfield, NY, USA) held 20 cm above and angled 45° relative to the soil surface; (2) measuring resistance of the soil to pocket penetrometers (QA Supplies, FT011) inserted 45° relative to the soil surface. The penetrometer measurement was recorded when the soil surface was breached. Six pocket penetrometer readings and two airgun readings were made per plot.

For chlorophyll *a* (chl *a*) and EPS, five ~ 2 g soil samples were taken from the top 1 cm of the soil surface at regularly spaced intervals along the diagonal of each plot. Individual collections were performed on a subset of these samples (two blocks or 24 plots), while the remaining extractions were performed on pooled samples for each plot. Chl *a* was extracted by grinding 1 g of soil with a mortar and pestle in 3 ml of 90% acetone for three minutes. The sample and solvent mixture were brought up to 10 ml with 90% acetone and the sample was vortexed for two minutes and incubated in the dark at 4 °C for 24 hours. After incubation, the sample was centrifuged for 12 minutes at 4000 RPM and 15 °C. The absorbance of the supernatant was recorded at 663 nm using an Ocean Optics CHEMUSB4-VIS-NIR spectrophotometer (400–950 nm) and at 1000 nm for background adjustment. We used the adjusted absorbance and soil sample mass to determine chl *a* content using calculations outlined in Ritchie (2006). EPS from colloidal and tightly-bound fractions were extracted and quantified following a modified version as described in De Brouwer and Stal (2001) using 50 mg soil samples, a 15 minute initial extraction time followed by vortexing and 8000 × *g* centrifugations. We also measured EPS of powdered psyllium soil stabilizer. Absorbances were read on an Ocean Optics CHEMUSB4-VIS-NIR spectrophotometer (400–950 nm) at 490 nm along with a 1000 nm background reading which subtracted as the baseline. This EPS extraction method measures all extracellular carbohydrates (including those from non-biocrust organisms). For brevity and simplicity, we refer to this collection of carbohydrates as EPS. As polysaccharides are a main constituent of the psyllium-based soil stabilizer added to plots (Fischer et al., 2004), we measured the EPS content of pure M-binder. We estimate that approximately 0.56 g of

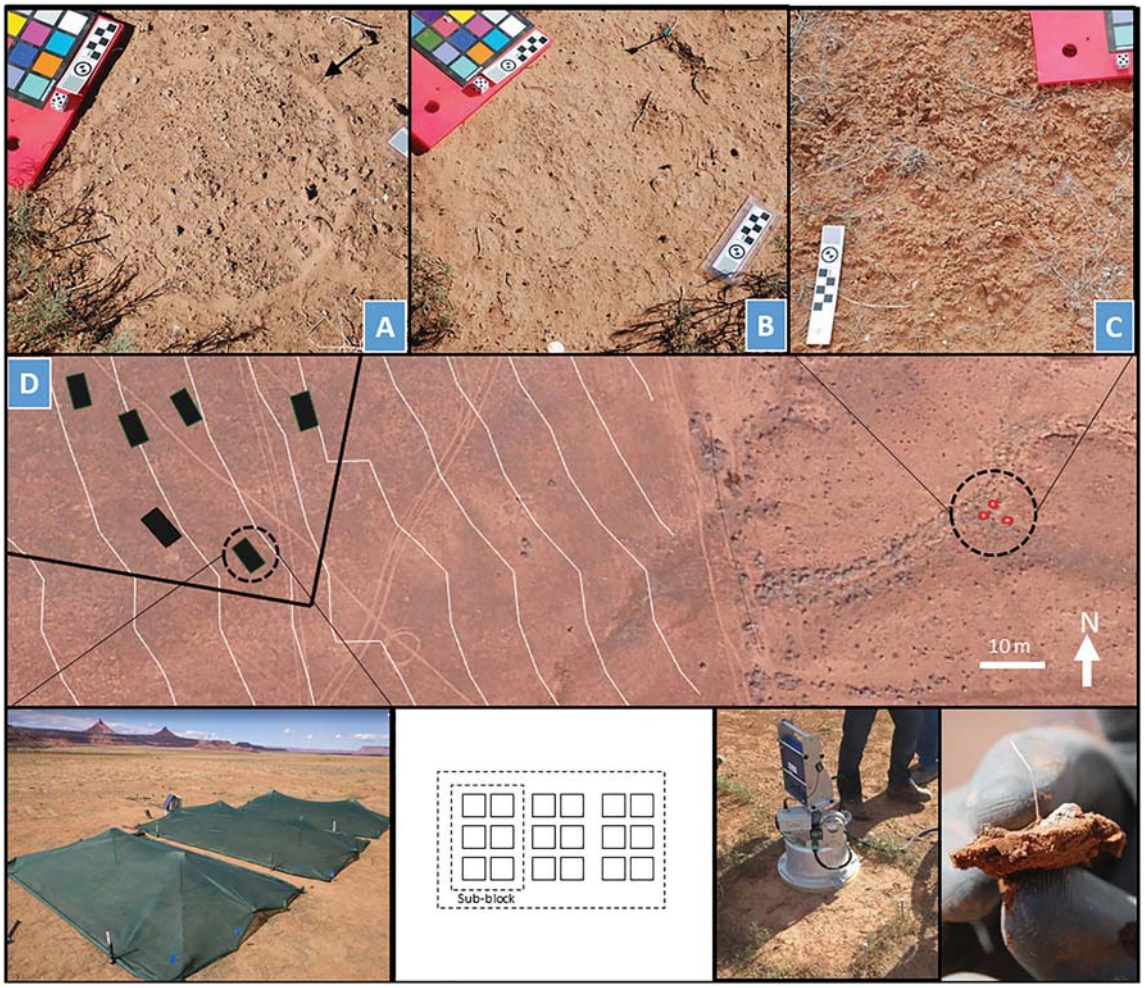

Figure 1. Study site and plot surfaces. (A) Typical biocrust-treated plot surface (40% inoculation rate) after sampling by the PI-SWERL. Note the buildup of displaced loose sediment around the perimeter of the PI-SWERL chamber's footprint (arrow). (B) Control plot adjacent to (A) after PI-SWERL sampling. Control plots lacked evidence of accumulated sediment following sampling. (C) Surface of reference biocrust plot. (D) Overview of experimental site. Dark rectangles represent blocks, red squares indicate reference plots, the thick black line indicates the fenceline, and parallel white lines indicate 0.5 m vertical topographic contours, following a slight southwest aspect. (E) Shading structures covering plots, installed mid-March 2018. (F) Plot layout. Each block contained three sub-blocks containing all treatments and covered by a single shade structure. The two distal sub-blocks (out of three) were sampled per block. (G) Mini PI-SWERL. (H) Biocrust surface plate removed at the end of the experiment (June 2018). [Colour figure can be viewed at wileyonlinelibrary.com]

equivalent detectable EPS were added per square meter at the outset of the experiment (1088 ± 61 ug g^{-1} loosely-bound, 8191 ± 429 ug g^{-1} tightly-bound).

In mid-June, five subsamples of the soil surface (top 1 cm) not exposed to PI-SWERL simulations were collected and then pooled for each plot and characterized to particle size using laser diffraction (Beckman Coulter LS 13 320, Brea, CA, USA). Samples were dispersed using a combination of sodium hexameta phosphate (50 g l^{-1}) with shaking overnight and further kept in suspension during analysis using sonication.

Wind erosion simulations

In early June, potential dust emissions at different simulated wind friction velocities were measured using a miniature portable in-situ wind erosion laboratory (Mini PI-SWERL, DustQuant LLC, Las Vegas, NV, USA) on undisturbed portions of each plot. The specifications and operation of the PI-SWERL has been described in detail elsewhere (Etyemezian et al., 2007; Kavouras et al., 2009). Briefly, the Mini PI-SWERL consists of an open-bottomed cylindrical chamber (26 cm diameter, 20 cm height) placed flush to the soil surface. The chamber is instrumented with a flat, rotating annular ring suspended 60 mm above the soil surface which generates surface shear stress proportional to the rotational velocity of the ring. During sampling, airflow into the chamber is carefully controlled and PM_{10} dust concentrations are continuously measured with a DustTrak nephelometer (TSI Inc. Shoreview, MN, USA), while activity of saltating particles is detected with two optical sensors mounted near the base of the chamber. Tests consisted of staged or 'stepped' exposures to incremental rotational velocities of 0, 2000, 3000, 4000 and 5000 RPM, with gradual increases in velocity between steps (Figure 2). The time of exposure to each step was maintained for 60 seconds, with approximately 45 seconds of acceleration between steps for a total sampling time of around 540 seconds. We did not determine the friction velocity for each revolution per minute (RPM) as affected by roughness according to Etyemezian et al. (2014). Rather we used the nominal friction velocities at each RPM as reported by Etyemezian et al. (2007) since the surface used in that study were more similar to our surfaces.

PM_{10} concentrations at each step were averaged to estimate mean flux as a function of the effective area exposed to shear stress directly under the annular ring (0.02 m^2). Occasional deviations in rotational velocity at each step were filtered from analysis by discarding any readings where observed RPM was less than 95% of target RPM.

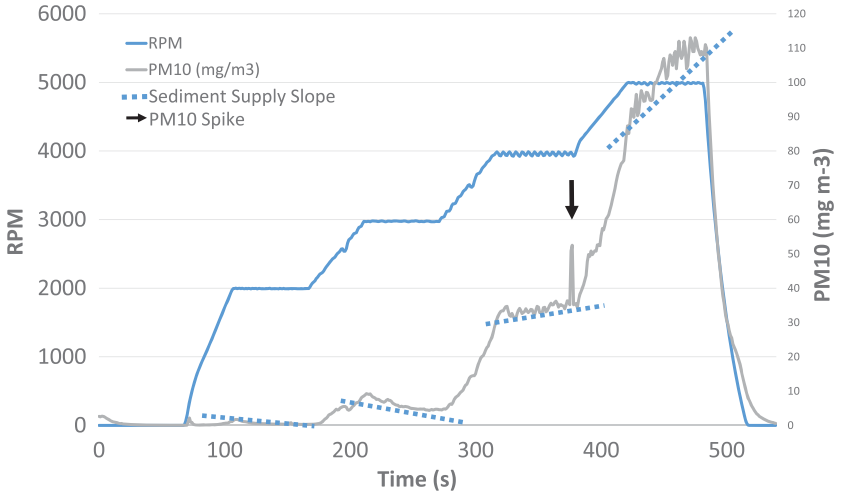

Figure 2. *Typical PI-SWERL run* output. PM_{10} emissions measured as soil surfaces are subjected to incrementally increasing shear stress from the rotation of an annular blade, with marked 'steps' at 0, 2000, 3000, 4000 and 5000 RPM. At step velocities, PM_{10} fluxes may decline, remain at equilibrium or increase, as indicated by the sediment supply slope. Occasionally spikes in PM_{10} may be observed (arrow), potentially corresponding to a detatched saltating particle. [Colour figure can be viewed at wileyonlinelibrary.com]

Instantaneous fluxes at different stepped rotations were not stable over time, and often trended downward (indicating exhaustion of mobile sediment supply) or upward (indicating increasing moveable sediment supply) (Figure 2). To quantify this effect, emissions for each step were standardized to zero-mean unit variance distributions and fit to linear models as a function of exposure time. The slope coefficients from these models were subsequently used in analysis to approximate whether sediment limitation was occurring.

TFV, indicating the wind velocity necessary to dislodge soil particles, is a common indicator of erodibility. To estimate TFV, the second derivative of cumulative PM_{10} emissions between steps was plotted against friction velocity to identify friction velocities where the 'slope' of emissions significantly diverged from the horizontal. These changes were represented as obvious local maxima in the second derivative of the accumulation curve, which were visually identified (Supporting Information Figure S1).

Occasional 'spikes' in PM_{10} emissions were observed during constant velocity exposures during simulations (Figure 2). To quantify the number of spikes per simulation, emissions time series at each step (except 0 RPM) were detrended by subtracting a smoothed-spline estimate from observed fluxes (using the R function smooth.spline with spar = 0.8). Local maxima exceeding 3.5 standard deviations of the de-trended mean were tallied as spikes (Figure S2). The first 10 seconds of each step were excluded from consideration to remove possible artifacts from annular blade acceleration.

Two sets of treatments were sampled with the PI-SWERL per block, resulting in a total of 78 erosion simulations, including the six reference plots. To compare friction velocities generated by the PI-SWERL to natural conditions, we estimated the long-term (15 years) distribution of friction velocities likely experienced on bare soil at the site. For all mean and maximum hourly windspeeds recorded at a climate station near (~3 km) the study site (Urban, 2017) friction velocities (U^*) were estimated using a logarithmic wind profile with a Von Kármán constant of 0.41, a displacement height of 0.1 m, and a roughness length of 0.03 m.

Analysis

Response variables at each stepped friction velocity, including average PM_{10} flux and emissions slope, as well as PM_{10} threshold friction velocity were modeled as a function of treatments and their interactions, with block included as a random effect. Prior to modeling, response variables were tested for normality with a Shapiro–Wilks test, and log transformed as appropriate. PM_{10} spikes were modeled with a generalized linear model using a Poisson error distribution with block as random effect and velocity step, stabilizer status and inoculation status (true/false) as predictors. Differences between modeled means of treatment group were tested with contrasts using the emmeans package (Lenth, 2018) in R (R Development Core Team, 2015), with a Tukey's HSD adjustment for multiple comparisons and alpha = 0.1.

To examine the plot-level parameters associated with simulated erosion responses, models were also fit using the full set of measured variables, including chl *a*, EPS, aggregate stability, standard deviation in aggregate stability, roughness index, pocket penetrometer resistance, physical crust cover, loose material cover, and biocrust cover, with block included as a random effect. Saturated models were subject to backward stepwise selection, removing the least significant parameter in turn until all parameters were significantly greater than zero, using a threshold of alpha = 0.1.

All models were fit with the lme4 package (Bates et al., 2015) in R and coefficient significance evaluated with *t*-tests using Satterthwaite's method for calculation of degrees of freedom in the package lmerTest (Kuznetsova et al., 2017).

Results

Treatment responses to wind simulations

Average PM_{10} flux increased exponentially with increasing friction velocity, and treatment differences were only apparent above friction velocities of 0.54 m s^{-1} (3000 RPM). This is consistent with Bagnold (1943) and Skidmore (1986) who found that particle movement rate above a certain threshold is directly proportional to friction velocity cubed. Increasing friction velocities amplified existing differences among treatments (Figures 3A and 3B), with plots only receiving the soil stabilizer having the greatest average flux of PM_{10} emissions. When soil stabilizer was combined with the highest level of biocrust inoculum (40%), emissions were the lowest among the treatments for high wind shear velocities (Figure 3A, with a significant interaction between inoculation and stabilizer, $p < 0.001$). These

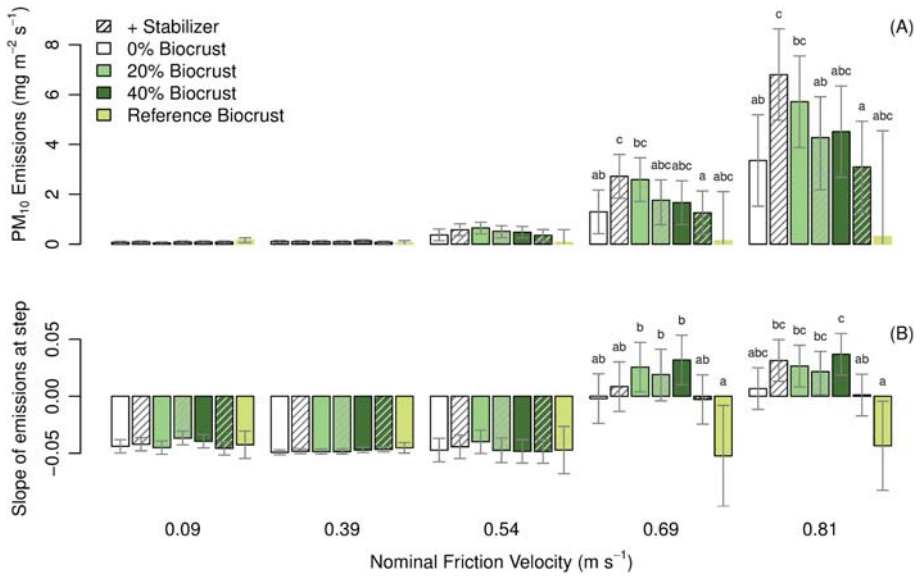

Figure 3. PM_{10} fluxes and emissions response slopes. (A) Average fluxes of measured PM_{10} emissions by treatment and friction velocity. (B) Sediment versus velocity limitation by treatment and friction velocity. Normalized slopes represent the tendency of PM_{10} emissions to either decay (negative slopes), grow (positive slopes) or maintain equilibrium (slopes = 0) when subjected to a constant friction velocity (the 'steps' in Figure 2). Nominal friction velocities correspond to 0, 2000, 3000, 4000, and 5000 RPM, respectively. Reference biocrust estimates based on three replicates. Vertical lines indicate ± 1 standard error, with significant differences among treatments (within friction velocities) indicated by differing letters. Hashed bars indicate addition of stabilizer. [Colour figure can be viewed at wileyonlinelibrary.com]

values, however, did not significantly differ from control plots. There was a marginally significant relationship between emissions at high shear velocities and inoculation rate ($p = 0.067$; with lower emissions at the higher inoculation rate; Figure 3A).

For periods of constant wind-shear stress ('steps' in Figure 2), sediment limitation was more apparent at low friction velocities, while sediment amplification was apparent at high friction velocities. This was evident in the transition from negative emissions slope coefficients to positive coefficients at high velocities (Figure 3B). Experimental treatment differences were only observed at friction velocities above 0.54 m s^{-1}. Only the treatment consisting of both high-inoculation rate and stabilizer showed any significant differences from others, exhibiting greater sediment limitation than the high-inoculum only plots (Figure 3B). The reference biocrust plot exhibited sediment limitation (negative slope coefficient) across all velocities.

The total number of PM_{10} spikes were nearly 75% greater in inoculated plots than uninoculated plots ($Z = 2.08$, $p = 0.0375$, Figure S3), but there were no effects of stabilizer or an interaction between stabilizer and inoculation. There were no significant differences among treatments for threshold friction velocity.

Relationships between surface indicators and erodibility

Soil surfaces were sandy loams (4–6% clay), with most of the textural variability occurring on a continuum of relative composition of sand to silt (between 50–65% sand and 45–30% silt, respectively). Treated plots were significantly sandier than controls (Figure 4, Table S2), by roughly 2%. This was likely because these plots had collected sand on the surface. Plots inoculated with biocrust had roughly two- to five-times higher levels of chl *a* than control, and slightly greater percentages of sand in surface sediments (Figure 4, Table S2). All treated plots had greater roughness and loose material cover than controls, with stabilizer-only plots having the greatest roughness and loose material cover (Figure 4, Table S2).

Stepwise model selection identified several biophysical variables which explained among plot variance in the soil erodibility responses from PI-SWERL simulations. Indicators of surface strength, including hand-held penetrometer resistance, projectile penetrometer resistance and EPS, tended to be associated with reduced erodibility across friction velocities (Figure 5). Similarly, surface cover by loose material and sand percentage in surface sediments tended to be associated with greater fluxes and lower TFV (Figure 5). While surface roughness was positively associated with TFV and reduction in fluxes at low friction velocities, it was associated with greater PM_{10} fluxes at high (5000 RPM) friction velocities (Figure 5). Sediment limitation was negatively associated with both hand-held penetrometer readings and chl *a* at low friction velocities (Figure 5). Aggregate stability was not identified as a significant predictor of erodibility metrics in model selection.

Discussion

Sediment accumulation and differences from control

There were no instances in which experimental treatments had significantly lower wind erodibility or emissions than control plots, and in some instances, treatments (either biocrust inoculum or soil stabilizer by themselves) yielded more emissions than the controls (Figure 3A). At the time of experimental simulation, control plot surfaces were nearly blank, with significantly less loose material cover and surface roughness (Figure 4). The small but significant differences in microtopography were associated with greater amounts of loose sediment cover on rougher plots ($\rho = 0.24$, $p = 0.012$, Figure 4), likely representing the accumulation of sediment driven by windy conditions in the spring (Figure S4). Furthermore, following wind erosion simulations, we observed a build-up of loose sediment around the circular perimeter of the PI-SWERL chamber in treated plots (Figure 1A), which was systematically absent from control plots (Figure 1B). Surface roughness elements can reduce erosive force, enabling

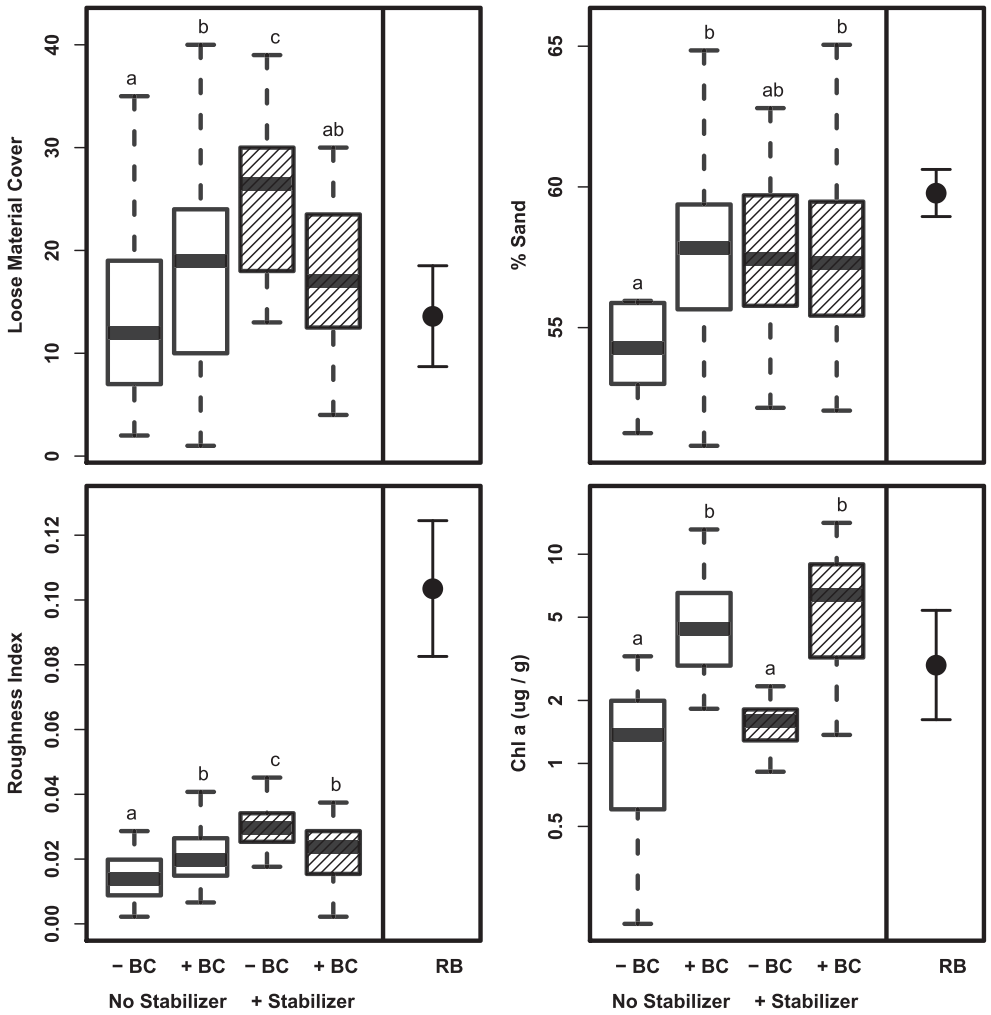

Figure 4. Average loose material surface cover, percent sand, roughness index, and chlorophyll *a* by treatment. Higher roughness index values indicate greater estimated surface micro-relief. Groups sharing lowercase letters are not significantly different, as based on pairwise comparisons of expected marginal means from a model including block as random effect. Range, interquartile range, and medians indicated by dashed lines, boxes, and heavy horizontal bars, respectively. Plots with biocrust addition indicated as (+BC) and without indicated by (–BC). The filled circle and bars represent the mean and standard error values for the reference biocrust plots (n = 3).

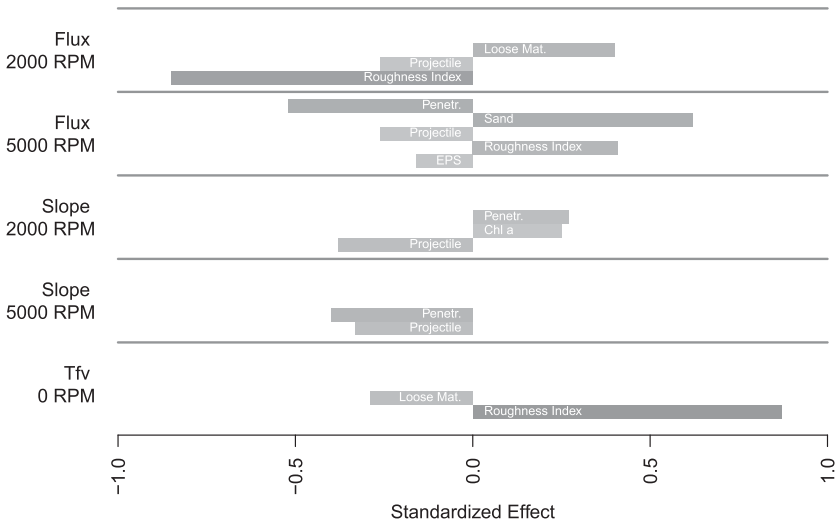

Figure 5. **F**actors significantly associated with erodibility. Standardized coefficients from stepwise model selection represented as shaded bars. Response variables tested include threshold friction velocity (TFV), the slope of emissions profiles at stepped PI-SWERL velocities (slope at 5000 and 2000 RPM), and emissions (flux at 5000 and 200 RPM). Factors include impact area from a projectile penetrometer (Projectile), resistance to hand held penetrometer (Penetr.), percent loose material surface cover (Loose Material), surface roughness index (Roughness Index), soil chlorophyll *a* concentration (Chl a), soil exopolysaccaride content (EPS) and percent sand in the top 1 cm of soil (Sand).

the build-up of dust and sediment (Goossens, 1995). While some of the greater erodibility observed in simulations for treated plots was likely due to induced differences in surface strength (e.g. higher tendency for crust detachment and PM_{10} 'spikes' in plots with biocrust, Figure S3), much of the apparent difference between control and treated plots may be explained by the difference in availability of loose sediment. Dust emissions have been strongly linked to bombardment of fine soil aggregates by saltating sand (Shao et al., 1993), and the greater supply of erodible sand particles in treatments may thus be partially responsible for observed PM_{10} flux differences.

Alternatively, the small differences in microtopographic roughness induced in treated plots may have contributed to greater PM_{10} fluxes, as has been observed in post-burn shrub microsites and interspaces (Sankey et al., 2011). While surface roughness can reduce erosion by decreasing net wind momentum (Gillette and Stockton, 1989), non-erodible roughness elements (e.g. rocks) at low densities can increase local erosive force via the scouring effect of leeward turbulent flow (Lee, 1991;Raupach et al., 1993 ; Neakrase and Greeley, 2010). The biocrust and stabilizer aggregates present in treated plots in this study occurred at relatively low densities (compare Figure 1A versus Figure 1C) and could have functioned in this way. Surface roughness elements generated within natural patches of biocrust are generally more dense and have greater net micro-relief (Figure 1C, Miller et al., 2011), making them less likely to induce particle movement (Raupach et al., 1993; Neakrase and Greeley, 2010).

In the present study, it is not possible to resolve the mechanisms responsible for elevated emissions observed in some treated plots (whether from eroding inoculum, accumulated loose sediment, or roughness-induced scouring). It is possible that all of the proposed mechanisms could be contributing to emissions to some degree. From a broader, landscape-scale perspective, the positive effect of trapping mobile sediment on rough surfaces (reducing net soil loss and particle bombardment) may compensate for local increases in emissions from roughness-induced scouring or other effects. In the spring of 2018, we observed mobile sediment from adjacent bare and actively grazed areas blowing across the study site (S. Fick, personal observation), which may have been preferentially trapped on treated plots, which were significantly more rough than controls (Figure 4). In many cases the accelerated sediment trapping by induced biocrusts may be a desirable function, with captured sediment and dust critical to soil-building and ecosystem productivity in the study area (Reynolds et al., 2001). Furthermore, short-term rises in emissions resulting from inoculation (which were mitigated by combining inoculum and soil stabilizer, discussed later), would likely decline with continued biocrust development, leading to more contiguous patches of roughness elements and lower expected emissions (biocrust reference, Figures 1C and 3).

The surface shear-velocities simulated by the PI-SWERL in this experiment are comparable to estimated friction velocity values found regionally (Figure 6). For relatively bare surfaces analogous to experimental plots, nearby wind station data suggest that hourly average friction velocities equal to or exceeding 0.69 m s^{-1}, the point at which treatment differences became apparent with the PI-SWERL data, occur approximately 3% of the time, and 26% of the time for maximum gusts per hour. Cumulatively, these levels of exposure could result in dramatically different levels of PM_{10} emissions for different stabilization treatments across the region, based on experimental data. However, given the discrepancy between fluxes from experimental plots and relatively undisturbed surfaces nearby (e.g. reference plots in Figure 4), experimental results from this study may be better interpreted as indices of short-term erosion

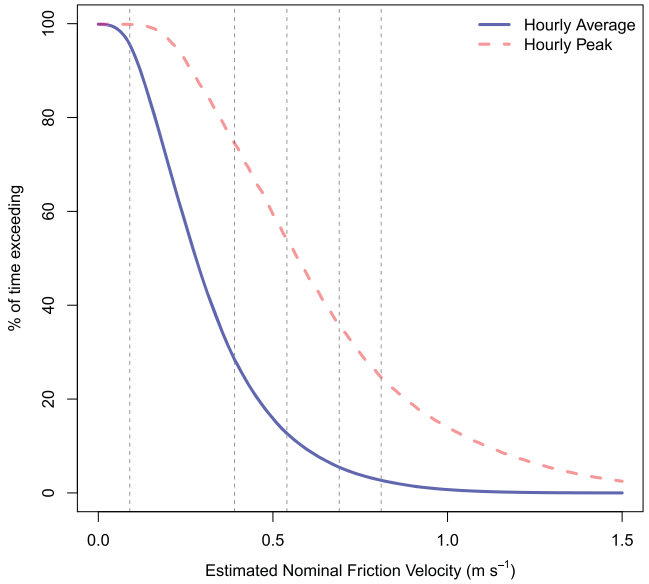

Figure 6. Estimated frequencies of friction velocities experienced in the study region over 20 years. Friction velocities (U^*) were estimated based on a logarithmic wind profile using a Von Kármán constant of 0.41, a displacement height of 0.1 m, and a roughness length of 0.03 m from mean and maximum hourly windspeeds recorded at 2 m from a climate station near (~3 km) the study site (Urban, 2017). Vertical dashed lines indicate the step friction velocities (at 0.09, 0.39, 0.54, 0.69, 0.81 m s^{-1}) generated by each PI-SWERL step. Average windshear velocities equal to or exceeding 0.69 m s^{-1}, the point at which flux estimates began to significantly differ by treatment in this study, occur approximately 3% and 26% of the time for average and peak wind velocities, respectively. [Colour figure can be viewed at wileyonlinelibrary.com]

responsiveness after biocrust induction, rather than means for quantifying long-term emissions.

Synergistic effects of biocrust inoculation and soil stabilizer

Surfaces receiving both soil stabilizer and inoculation of biocrust generally exhibited lower rates of emissivity than surfaces with either of these treatments alone across emissions-related response variables, especially at high friction velocities (Figures 3 and 7). There are a number of potential explanations as to why a mixture of inoculum and stabilizer would have greater resistance to wind shear stress. First, the sediment from the biocrust particles in the mixed treatments may have helped distribute the stabilizer across the plot surface, providing better contact between the polymers of the soil binder and mineral soil particles. It was observed in the stabilizer-only treatments that the compound tended to clump and adhere to itself after initial application, later forming thin flakes and plates poorly anchored to the soil surface. These features are likely responsible for the greater roughness values observed in stabilizer-only plots (Figure 4). During high velocity step treatments from the PI-SWERL these flakes may have detached and increased emissions rates by colliding with other soil particles (Figure 2). Plots with both stabilizer and biocrust did not have observable flaking features. Second, the psyllium stabilizer may have promoted the stability and growth of biocrust during the experiment. Wind velocities observed near the site during the growth phase were greater than average (Figure S4; USGS Clim-met data, Urban, 2017), and the stabilizer may have served to anchor biocrust aggregates during development and during the experimental wind simulation. In a parallel rainfall

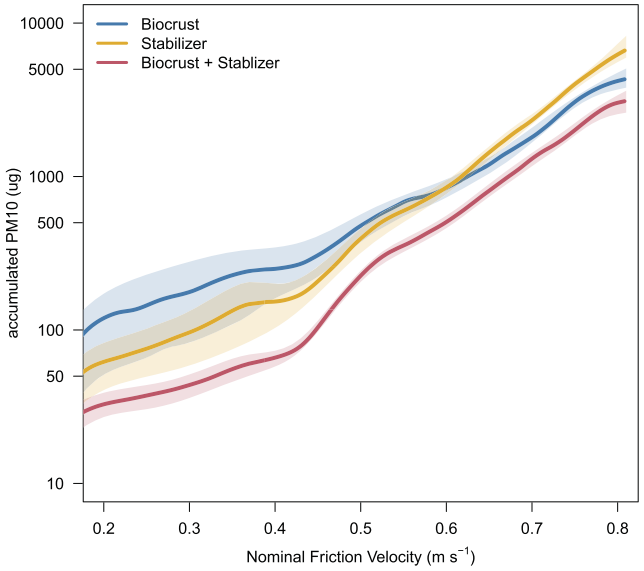

Figure 7. Average PM_{10} accumulations by treatment and friction velocity ± one standard error. Accumulation curves were derived from accelerating conditions in PI-SWERL experiments (i.e. excluding the 'stepped' values). Here biocrust indicates results from the maximum inoculum dose applied (40%). [Colour figure can be viewed at wileyonlinelibrary.com]

simulation experiment (Fick et al., 2019), loose particles from biocrust inoculation were implicated in higher sediment yields, but this trend was ameliorated when stabilizer was added. The gelatinous nature of the stabilizer itself may have promoted the development of cyanobacterial filaments by providing interstitial 'bridges' among coarse sand particles (e.g. Park et al., 2014; Zaady et al., 2016), and potentially buffering osmotic or nutritional stress during growth (Park et al., 2016). Levels of soil chl *a* (a proxy for cyanobacterial growth, Figure 4), as well as aggregate stability were highest on average in plots with both high inoculation rates and stabilizer (data not shown).

The cumulative effects of these treatments suggest that combinations of inoculation and soil stabilizer reduce net PM_{10} emissions by a factor of two (Figure 6), at least after the short duration of this experiment (four months). Other studies using combinations of stabilizers and inoculation have found similar results in the laboratory and over longer periods in the field (Park et al., 2017), and yet others have found null results over even longer timespans up to 10 years (Chandler et al., 2018). The choice of stabilizer is likely an important factor for the efficacy of these treatments, due to potential interactions with biocrust biology, and the period over which the stabilizer degrades.

Correlates of erodibility

Variables related to surface strength (including EPS, projectile, and hand-held penetrometer resistance) were generally strong correlates of resistance to wind erosion across friction velocities (as identified in stepwise model selection; Figure 5). Working in nearby sites on the Colorado Plateau, Li et al. (2010) were able to approximate wind-tunnel-derived TFV using linear combinations of pocket and projectile penetrometer readings, achieving a high correspondence (R^2 = 0.9). We found much poorer correspondence between TFV and these measurements using the equations published in Li et al. (2010) in this study (ρ = 0.10, Table S3). However, we used a different method to estimate TFV (see Sweeney et al. (2008) for a comparison of PI-SWERL and wind-tunnel results) and we did not detect any treatment-related differences in TFV for our study. We did find modest correlations between TFV approximated using the Li et al. (2010) method and emissions at high friction velocities, reinforcing the utility of these measurements as quick approximations of erosion resistance.

Positive relationships between measures of surface integrity, biocrust biomass, and resistance to erosion have been found in other wind erosion simulations (Belnap and Gillette, 1997; Eldridge and Leys, 2003; Belnap et al., 2007; Park et al., 2017). Much of the erosion-resistance in biocrusts is attributed to the soil-binding activity of EPS and biocrust filaments, which are particularly important for maintaining integrity in cyanobacterially-dominated soils (Williams et al., 1995; McKenna-Neuman et al., 1996; Kidron et al., 2017). Interestingly, while chl *a* and aggregate stability were both negatively associated with emissions at high RPMs (Table S4) in this study, they were not selected in model stepwise selection, indicating they were not dominant predictors of emissions, considering other factors. Rather, a combination of physical surface strength and surface texture values were found to be the most parsimonious predictors, highlighting the complexity and context dependency of erosion processes (Okin et al., 2006; Belnap et al., 2007). While measures such as aggregate stability and chl *a* may suffice as coarse proxy measurements for erodibililty, absent simulations, care should be taken extrapolating these values as direct estimates.

Both loose material and sand concentrations were positively associated with fluxes, consistent with other findings which link sand content and dust emissions (Sweeney et al., 2008, 2011). Roughness was found to be positively associated with threshold friction velocity and negatively associated with PM_{10} flux at low friction velocities, as expected (Figure 5). Yet at higher friction velocities, roughness was associated with greater fluxes (also seen in Figure 6). This may be related to trapped sediment becoming dislodged at higher velocities, as well as breakage and flaking of biocrust and stabilizer amendments (Figure 3, McKenna-Neuman et al., 1996). Although moderate levels of biocrust development were observed in the short time of this study, they differ from well-developed erosion-resistant biocrusts found in the area which have greater amounts of biomass and surface roughness (Figure 4). It is likely that given more time for development, inoculated surfaces would increase resistance to erosion and approach levels observed in reference biocrust plots (Belnap et al., 2008).

Interestingly, both chl *a*, an indicator of biocrust organism growth, and hand-held penetrometer resistance were negatively associated with sediment limitation (i.e. associated with a more-positive emissions slope) at low friction velocities (Figure 5). Given the fact that nearly all emissions slopes were negative at 2000 RPM, more positive slopes (closer to zero) may indicate either lack of appreciable material to deplete or slower depletion of available material during the simulation. This ambiguity may drive the unexpected result of the two surface tensile strength metrics having opposite signs (likely reflecting collinearity in these variables).

Methods for evaluating PI-SWERL data

Wind simulation studies have documented the transition from supply-limited to sustained effluxes following surface crust deterioration (Chepil, 1951; Chepil and Woodruff, 1963; McKenna Neuman et al., 2005). PI-SWERL data enables interpretation of these events (Sankey et al., 2012; Sweeney and Mason, 2013), and in this study quantification of the slope of PM_{10} emissions at various stepped rotational velocities was an indicator of surface strength that clearly mirrored the pattern

in average flux (Figure 2), with slightly more nuanced differences between treatments and a relatively clear physical interpretation (Sweeney et al., 2008). The point at which the slope of emissions transitioned from limitation (declining slope) to acceleration (increasing slope) is an important threshold for characterizing surfaces, beyond TFV. The variability and generality of patterns in emissions slopes could be explored across a wider set of soil types and contexts, even with existing PI-SWERL data.

To our knowledge, the quantification PM_{10} spikes is a relatively novel application of PI-SWERL timeseries data. Enumeration of PM_{10} spikes could be useful for characterizing surfaces, potentially indicating the effects of fragmentation and movement of large surface particles, as it was in this study. However, the DustTrak sensors in the PI-SWERL are known to produce spurious noise, and controlled studies are needed to verify causal mechanisms of PM_{10} spikes before the general application of this methodology.

Conclusions

Inducing biocrust development remains an appealing restoration activity in drylands, not least because of the long-lasting resistance biocrusts provide against wind erosion and dust emissions. As knowledge and technology coalesce to improve the efficiency of biocrust-mediated dust mitigation, it is important to quantify the ecosystem impacts and timescales associated with biocrust development. We found that biocrust inoculation, especially when combined with a soil stabilizer, began to confer sediment-accumulating benefits within the short period of this experiment (four months), and yielded dust emissions statistically indistinguishable from bare controls. The induced biocrusts in this experiment differed notably from undisturbed biocrusts in terms of surface roughness, although with more time and exposure to freeze–thaw cycles through winter it is likely that the experimental biocrusts would develop the microtopography that is characteristic of biocrusts in the region. Further investigations into the mechanisms by which soil stabilizer and biocrust inoculation interact are warranted in order to design successful biocrust restoration strategies as well as expand our understanding of biocrust biology.

Acknowledgments—This project was supported by the Strategic Environmental Research and Development Program (SERDP RC-2329) and the US Geological Survey Ecosystems Mission Area. The authors thank the following people for help with fieldwork and laboratory work: Scott Van Pelt, Chunping Chang, Hilda Smith, Sean Hoy-Skubic, Jessica Mikenas, Sabine Nix, Madeline Moore, Alexander Sandberg-Bernard, Lior Gross, Karin Dove, and Brian Fick. Any use of trade, product, or firm names is for descriptive purposes only and does not imply endorsement by the US Government.

References

Antoninka A, Bowker MA, Chuckran P, Barger NN, Reed S, Belnap J. 2017. Maximizing establishment and survivorship of field-collected and greenhouse-cultivated biocrusts in a semi-cold desert. *Plant and Soil* **429**(1-2): 213–225. https://doi.org/10.1007/s11104-017-3300-3

Antoninka A, Bowker MA, Reed SC, Doherty K. 2015. Production of greenhouse-grown biocrust mosses and associated cyanobacteria to rehabilitate dryland soil function. *Restoration Ecology* **24**(3): 324–335. https://doi.org/10.1111/rec.12311

Armbrust D, Lyles L. 1975. Soil stabilizers to control wind erosion. In *Soil Conditioners*, Soil Science Society of America, Special Publication No. 7. Soil Science Society of America: Madison, WI; 77–82.

Bagnold RA. 1943. *The Physics of Blown Sand and Desert Dunes*. William Morrow & Co.: New York.

Bates D, Mächler M, Bolker B, Walker S. 2015. Fitting linear mixed-effects models using lme4. *Journal of Statistical Software* **67**(1): 1–48. https://doi.org/10.18637/jss.v067.i01

Belnap J. 1993. Recovery rates of cryptobiotic crusts: inoculant use and assessment methods. *The Great Basin Naturalist* **53**(1): 89–95.

Belnap J. 2003a. Comparative structure of physical and biological soil crusts. In *Biological Soil Crusts: Structure, Function, and Management*, Belnap J, Lange OL (eds). Springer: Berlin; 177–191.

Belnap J. 2003b. Biological soil crusts and wind erosion. In *Biological Soil Crusts: Structure, Function, and Management*, Belnap J, Lange OL (eds). Springer: Berlin; 339–347. http://link.springer.com/chapter/10.1007/978-3-642-56475-8_25

Belnap J, Büdel B. 2016. Biological soil crusts as soil stabilizers. In *Biological Soil Crusts: An Organizing Principle in Drylands*. Springer: Berlin; 305–320.

Belnap J, Büdel B, Lange OL. 2003. Biological soil crusts: characteristics and distribution. In *Biological Soil Crusts: Structure, Function, and Management*, Belnap J, Lange OL (eds). Springer: Berlin; 3–30. http://link.springer.com/chapter/10.1007/978-3-642-56475-8_1

Belnap J, Eldridge D. 2003. Disturbance and recovery of biological soil crusts. In *Biological Soil Crusts: Structure, Function, and Management*, Belnap J, Lange OL (eds). Springer: Berlin; 363–383.

Belnap J, Gillette D. 1998. Vulnerability of desert biological soil crusts to wind erosion: the influences of crust development, soil texture, and disturbance. *Journal of Arid Environments* **39**(2): 133–142. https://doi.org/10.1006/jare.1998.0388

Belnap J, Gillette DA. 1997. Disturbance of biological soil crusts: impacts on potential wind erodibility of sandy desert soils in southeastern Utah. *Land Degradation & Development* **8**(4): 355–362.

Belnap J, Lange OL (eds). 2003. *Biological Soil Crusts: Structure, Function, and Management*. Springer: Berlin. https://doi.org/10.1007/978-3-642-56475-8

Belnap J, Phillips SL, Herrick J, Johansen J. 2007. Wind erodibility of soils at Fort Irwin, California (Mojave Desert), USA, before and after trampling disturbance: implications for land management. *Earth Surface Processes and Landforms* **32**(1): 75–84.

Belnap J, Phillips SL, Witwicki DL, Miller ME. 2008. Visually assessing the level of development and soil surface stability of cyanobacterially dominated biological soil crusts. *Journal of Arid Environments* **72**(7): 1257–1264.

Belnap J, Reynolds RL, Reheis MC, Phillips SL, Urban FE, Goldstein HL. 2009. Sediment losses and gains across a gradient of livestock grazing and plant invasion in a cool, semi-arid grassland, Colorado Plateau, USA. *Aeolian Research* **1**(1-2): 27–43.

Bowker MA. 2007. Biological soil crust rehabilitation in theory and practice: an underexploited opportunity. *Restoration Ecology* **15**(1): 13–23.

Chandler DG, Day N, Madsen MD, Belnap J. 2018. Amendments fail to hasten biocrust recovery or soil stability at a disturbed dryland sandy site. *Restoration Ecology* **27**(2): 289–297. https://doi.org/10.1111/rec.12870

Chepil W. 1951. Properties of soil which influence wind erosion: V. Mechanical stability of structure. *Soil Science* **72**(6): 465–478.

Chepil W, Woodruff N. 1963. The Physics of Wind Erosion and its Control 1. *Advances in Agronomy* **15**: 211–302.

Chiquoine LP, Abella SR, Bowker MA. 2016. Rapidly restoring biological soil crusts and ecosystem functions in a severely disturbed desert ecosystem. *Ecological Applications* **26**(4): 1260–1272.

Chock T, Antoninka AJ, Faist AM, Bowker MA, Belnap J, Barger NN .2019. Responses of biological soil crusts to rehabilitation strategies. *Journal of arid environments* **163**: 77–85.

De Brouwer JFC, Stal LJ. 2001. Short-term dynamics in microphytobenthos distribution and associated extracellular carbohydrates in surface sediments of an intertidal mudflat. *Marine Ecology Progress Series* **218**: 33–44.

Doherty KD, Antoninka AJ, Bowker MA, Ayuso SV, Johnson NC. 2015. A novel approach to cultivate biocrusts for restoration and experimentation. *Ecological Restoration* **33**(1): 13–16.

Duniway MC, Nauman TW, Johanson JK, Green S, Miller ME, Williamson JC, Bestelmeyer BT. 2016. Generalizing ecological site concepts of the Colorado Plateau for landscape-level applications. *Rangelands* **38**(6): 342–349. https://doi.org/10.1016/j.rala.2016.10.010

Duniway MC, Palmquist E, Miller ME. 2015. Evaluating rehabilitation efforts following the Milford Flat Fire: successes, failures, and controlling factors. *Ecosphere* **6**(5): 80. https://doi.org/10.1890/ES14-00318.1

Duniway MC, Pfennigwerth AA, Fick SE, Nauman TW, Belnap J, Barger NN. 2019. Wind erosion and dust from US drylands: a review of causes, consequences, and solutions in a changing world. *Ecosphere* **10**(3): e02650.

Eldridge DJ, Leys JF. 2003. Exploring some relationships between biological soil crusts, soil aggregation and wind erosion. *Journal of Arid Environments* **53**(4): 457–466.

Etyemezian V, Gillies J, Shinoda M, Nikolich G, King J, Bardis A. 2014. Accounting for surface roughness on measurements conducted with PI-SWERL: evaluation of a subjective visual approach and a photogrammetric technique. *Aeolian Research* **13**: 35–50.

Etyemezian V, Nikolich G, Ahonen S, Pitchford M, Sweeney M, Purcell R, Gillies J, Kuhns H. 2007. The portable in situ wind erosion laboratory (PI-SWERL): a new method to measure PM10 windblown dust properties and potential for emissions. *Atmospheric Environment* **41**(18): 3789–3796.

Fick SE, Barger N, Duniway M. 2019. Hydrologic function of rapidly induced biocrusts. *Ecohydrology* **7**: e2089.

Fick SE, Decker C, Duniway MC, Miller ME. 2016. Small-scale barriers mitigate desertification processes and enhance plant recruitment in a degraded semiarid grassland. *Ecosphere* **7**(6): e01354. https://doi.org/10.1002/ecs2.1354

Fischer MH, Yu N, Gray GR, Ralph J, Anderson L, Marlett JA. 2004. The gel-forming polysaccharide of psyllium husk (*Plantago ovata* Forsk). *Carbohydrate Research* **339**(11): 2009–2017.

Gillette DA, Stockton PH. 1989. The effect of nonerodible particles on wind erosion of erodible surfaces. *Journal of Geophysical Research: Atmospheres* **94**(D10): 12885–12893.

Gonzales HB, Ravi S, Li J, Sankey JB. 2018. Ecohydrological implications of aeolian sediment trapping by sparse vegetation in drylands. *Ecohydrology* **11**(7): e1986.

Goossens D. 1995. Field experiments of aeolian dust accumulation on rock fragment substrata. *Sedimentology* **42**(3): 391–402.

Griffin DW, Kellogg CA, Shinn EA. 2001. Dust in the wind: long range transport of dust in the atmosphere and its implications for global public and ecosystem health. *Global Change and Human Health* **2**(1): 20–33.

Herrick JE, Van Zee JW, Havstad KM, Burkett LM, Whitford WG. 2005. *Monitoring Manual for Grassland, Shrubland and Savanna Ecosystems. Volume I: Quick Start. Volume II: Design, Supplementary Methods and Interpretation*. USDA-ARS Jornada Experimental Range. USDA-ARS: Fort Collins, CO. Retrieved from http://www.cabdirect.org/abstracts/20053169289.html

Hu C, Liu Y, Song L, Zhang D. 2002. Effect of desert soil algae on the stabilization of fine sands. *Journal of Applied Phycology* **14**(4): 281–292. https://doi.org/10.1023/a:1021128530086

Huang J, Yu H, Guan X, Wang G, Guo R. 2016. Accelerated dryland expansion under climate change. *Nature Climate Change* **6**(2): 166.

Jia RL, Li XR, Liu LC, Gao YH, Li XJ. 2008. Responses of biological soil crusts to sand burial in a revegetated area of the Tengger Desert, Northern China. *Soil Biology and Biochemistry* **40**(11): 2827–2834.

Kavouras IG, Etyemezian V, Nikolich G, Gillies J, Sweeney M, Young M, Shafer D. 2009. A new technique for characterizing the efficacy of fugitive dust suppressants. *Journal of the Air & Waste Management Association* **59**(5): 603–612. https://doi.org/10.3155/1047-3289.59.5.603

Kidron GJ, Vonshak A, Abeliovich A. 2009. Microbiotic crusts as biomarkers for surface stability and wetness duration in the Negev Desert. *Earth Surface Processes and Landforms* **34**(12): 1594–1604.

Kidron GJ, Ying W, Starinsky A, Herzberg M. 2017. Drought effect on biocrust resilience: high-speed winds result in crust burial and crust rupture and flaking. *Science of the Total Environment* **579**: 848–859.

Kidron GJ, Zohar M. 2014. Wind speed determines the transition from biocrust-stabilized to active dunes. *Aeolian Research* **15**: 261–267.

Kuznetsova A, Brockhoff PB, Christensen RHB. 2017. lmerTest package: tests in linear mixed effects models. *Journal of Statistical Software* **82**(13): 1–26. https://doi.org/10.18637/jss.v082.i13

Larney FJ, Angers DA. 2012. The role of organic amendments in soil reclamation: a review. *Canadian Journal of Soil Science* **92**(1): 19–38.

Lee JA. 1991. Near-surface wind flow around desert shrubs. *Physical Geography* **12**(2): 140–146.

Lenth R. 2018. emmeans: Estimated Marginal Means, aka Least-Squares Means. [R package version 1.3.1]. Retrieved from https://CRAN.R-project.org/package=emmeans

Leys JF, Eldridge DJ. 1998. Influence of cryptogamic crust disturbance to wind erosion on sand and loam rangeland soils. *Earth Surface Processes and Landforms* **23**(11): 963–974.

Li J, Kandakji T, Lee JA, Tatarko J, Blackwell J, III, Gill TE, Collins JD. 2018. Blowing dust and highway safety in the southwestern United States: characteristics of dust emission "hotspots" and management implications. *Science of the Total Environment* **621**: 1023–1032.

Li J, Okin GS, Herrick JE, Belnap J, Munson SM, Miller ME. 2010. A simple method to estimate threshold friction velocity of wind erosion in the field: estimate threshold friction velocity. *Geophysical Research Letters* **37**(10): 1–5. https://doi.org/10.1029/2010GL043245

Li XR, Xiao HL, He MZ, Zhang JG. 2006. Sand barriers of straw checkerboards for habitat restoration in extremely arid desert regions. *Ecological Engineering* **28**(2): 149–157. https://doi.org/10.1016/j.ecoleng.2006.05.020

Li X-Y, Liu L-Y, Gong J-D. 2001. Influence of pebble mulch on soil erosion by wind and trapping capacity for windblown sediment. *Soil and Tillage Research* **59**(3-4): 137–142.

Lyles L, Schrandt R, Schmeidler N. 1974. Commercial soil stabilizers for temporary wind-erosion control. *Transactions of the ASAE* **17**: 134–139.

Mazor G, Kidron GJ, Vonshak A, Abeliovich A. 1996. The role of cyanobacterial exopolysaccharides in structuring desert microbial crusts. *FEMS Microbiology Ecology* **21**(2): 121–130. https://doi.org/10.1111/j.1574-6941.1996.tb00339.x

McKenna Neuman C, Maxwell C, Rutledge C. 2005. Spatial and temporal analysis of crust deterioration under particle impact. *Journal of Arid Environments* **60**(2): 321–342.

McKenna Neuman C, Maxwell CD, Boulton JW. 1996. Wind transport of sand surfaces crusted with photoautotrophic microorganisms. *Catena* **27**(3-4): 229–247. https://doi.org/10.1016/0341-8162(96)00023-9

Middleton N. 2017. Desert dust hazards: a global review. *Aeolian Research* **24**: 53–63.

Middleton N, Kang U. 2017. Sand and dust storms: impact mitigation. *Sustainability* **9**(6): 1053.

Miller ME, Belote RT, Bowker MA, Garman SL. 2011. Alternative states of a semiarid grassland ecosystem: implications for ecosystem services. *Ecosphere* **2**(5): art55. https://doi.org/10.1890/ES11-00027.1

Miller ME, Bowker MA, Reynolds RL, Goldstein HL. 2012. Post-fire land treatments and wind erosion – lessons from the Milford Flat Fire, UT, USA. *Aeolian Research* **7**: 29–44. https://doi.org/10.1016/j.aeolia.2012.04.001

Monsen SB, Stevens R, Shaw NL. 2004. *Restoring Western Ranges and Wildlands*, (No. Gen. Tech. Rep. RMRS-GTR-136-vol-1), US Department of Agriculture, Forest Service. Rocky Mountain Research Station: Fort Collins, CO; 294.

Nauman TW, Duniway MC, Webb NP, Belnap J. 2018. Elevated aeolian sediment transport on the Colorado Plateau, USA: the role of grazing, vehicle disturbance, and increasing aridity. *Earth Surface Processes and Landforms* **43**: 2897–2914.

Neakrase LD, Greeley R. 2010. Dust devils in the laboratory: Effect of surface roughness on vortex dynamics. *Journal of Geophysical Research: Planets* **115**(E5): 1–10.

Neff JC, Ballantyne AP, Farmer GL, Mahowald NM, Conroy JL, Landry CC, Overpeck JT, Painter TH, Lawrence CR, Reynolds RL. 2008. Increasing eolian dust deposition in the western United States linked to human activity. *Nature Geoscience* **1**(3): 189–195. https://doi.org/10.1038/ngeo133

Okin GS, Gillette DA, Herrick JE. 2006. Multi-scale controls on and consequences of aeolian processes in landscape change in arid and semi-arid environments. *Journal of Arid Environments* **65**(2): 253–275. https://doi.org/10.1016/j.jaridenv.2005.06.029

Okin GS, Parsons AJ, Wainwright J, Herrick JE, Bestelmeyer BT, Peters DC, Fredrickson EL. 2009. Do changes in connectivity explain desertification? *BioScience* **59**(3): 237–244.

Painter TH, Barrett AP, Landry CC, Neff JC, Cassidy MP, Lawrence CR, McBride KE, Farmer GL. 2007. Impact of disturbed desert soils on duration of mountain snow cover. *Geophysical Research Letters* **34**(12): 1–6. https://doi.org/10.1029/2007GL030284

Park C-H, Li X, Jia RL, Hur J-S. 2014. Effects of superabsorbent polymer on cyanobacterial biological soil crust formation in laboratory. *Arid Land Research and Management* **29**(1): 55–71. https://doi.org/10.1080/15324982.2014.928835

Park C-H, Li X-R, Jia R-L, Hur J-S. 2016. Combined application of cyanobacteria with soil fixing chemicals for rapid induction of biological soil crust formation. *Arid Land Research and Management* **31**(1): 81–93. https://doi.org/10.1080/15324982.2016.1198842

Park C-H, Li XR, Zhao Y, Jia RL, Hur J-S. 2017. Rapid development of cyanobacterial crust in the field for combating desertification. *PLOS One* **12**(6): e0179903. https://doi.org/10.1371/journal.pone.0179903

Peng C, Zheng J, Huang S, Li S, Li D, Cheng M, Liu Y. 2017. Application of sodium alginate in induced biological soil crusts: enhancing the sand stabilization in the early stage. *Journal of Applied Phycology* **29**(3): 1421–1428. https://doi.org/10.1007/s10811-017-1061-2

Pimentel D, Harvey C, Resosudarmo P, Sinclair K, Kurz D, McNair M, Crist S, Shpritz L, Fitton L, Saffouri R, others. 1995. Environmental and economic costs of soil erosion and conservation benefits. *Science* **267**: 1117–1123.

Poitras TB, Villarreal ML, Waller EK, Nauman TW, Miller ME, Duniway MC. 2018. Identifying optimal remotely-sensed variables for ecosystem monitoring in Colorado Plateau drylands. *Journal of Arid Environments* **153**: 76–87. https://doi.org/10.1016/j.jaridenv.2017.12.008

R Development Core Team. 2015. R: A Language and Environment for Statistical Computing. R Foundation for Statistical Computing: Vienna. Retrieved from ftp://155.232.191.133/cran/doc/manuals/r-devel/R-lang.pdf

Raupach M, Gillette D, Leys J. 1993. The effect of roughness elements on wind erosion threshold. *Journal of Geophysical Research: Atmospheres* **98**(D2): 3023–3029.

Ravi S, D'odorico P, Breshears DD, Field JP, Goudie AS, Huxman TE, Li J, Okin GS, Swap RJ, Thomas AD, others. 2011. Aeolian processes and the biosphere. *Reviews of Geophysics* **49**(3): 1–45.

Reheis MC, Urban FE. 2011. Regional and climatic controls on seasonal dust deposition in the southwestern US. *Aeolian Research* **3**(1): 3–21.

Reynolds JF, Smith DMS, Lambin EF, Turner BL, Mortimore M, Batterbury SP, Downing TE, Dowlatabadi H, Fernández RJ, Herrick JE. 2007. Global desertification: building a science for dryland development. *Science* **316**(5826): 847–851.

Reynolds R, Belnap J, Reheis M, Lamothe P, Luiszer F. 2001. Aeolian dust in Colorado Plateau soils: nutrient inputs and recent change in source. *Proceedings of the National Academy of Sciences* **98**(13): 7123–7127.

Ritchie RJ. 2006. Consistent sets of spectrophotometric chlorophyll equations for acetone, methanol and ethanol solvents. *Photosynthesis Research* **89**(1): 27–41.

Saleh A. 1993. Soil roughness measurement: chain method. *Journal of Soil and Water Conservation* **48**(6): 527–529.

Sankey JB, Eitel JU, Glenn NF, Germino MJ, Vierling LA. 2011. Quantifying relationships of burning, roughness, and potential dust emission with laser altimetry of soil surfaces at submeter scales. *Geomorphology* **135**(1-2): 181–190.

Sankey JB, Germino MJ, Glenn NF. 2012. Dust supply varies with sagebrush microsites and time since burning in experimental erosion events. *Journal of Geophysical Research: Biogeosciences* **117**(G1): 1–13.

Sankey JB, Wallace CS, Ravi S. 2013. Phenology-based, remote sensing of post-burn disturbance windows in rangelands. *Ecological Indicators* **30**: 35–44.

Seybold C, Herrick J. 2001. Aggregate stability kit for soil quality assessments. *Catena* **44**(1): 37–45.

Shao Y, Raupach M, Findlater P. 1993. Effect of saltation bombardment on the entrainment of dust by wind. *Journal of Geophysical Research: Atmospheres* **98**(D7): 12719–12726.

Skidmore E. 1986. Wind erosion climatic erosivity. *Climatic Change* **9**(1-2): 195–208.

Sweeney M, Etyemezian V, Macpherson T, Nickling W, Gillies J, Nikolich G, McDonald E. 2008. Comparison of PI-SWERL with dust emission measurements from a straight-line field wind tunnel. *Journal of Geophysical Research* **113**(F1); 1–12. https://doi.org/10.1029/2007JF000830

Sweeney MR, Mason JA. 2013. Mechanisms of dust emission from Pleistocene loess deposits, Nebraska, USA. *Journal of Geophysical Research: Earth Surface* **118**(3): 1460–1471.

Sweeney MR, McDonald EV, Etyemezian V. 2011. Quantifying dust emissions from desert landforms, eastern Mojave Desert, USA. *Geomorphology* **135**(1-2): 21–34.

Thomas AD, Dougill AJ. 2007. Spatial and temporal distribution of cyanobacterial soil crusts in the Kalahari: implications for soil surface properties. *Geomorphology* **85**(1-2): 17–29.

UNEP, WMO, and UNCCD. 2016. *Global Assessment of Sand and Dust Storms*, (No. DEW/1971/NA). United Nations Environment Programme (UNEP): Nairobi.

Urban FE. 2017. *Climate Impact Meteorological Stations (CLIM-MET) Data from The Mojave National Preserve, California and Canyonlands National Park, Utah 1998-2016*, US Geological Survey data release. US Geological Survey: Reston, VA. Retrieved from https://doi.org/10.5066/F76H4GBF

US Department of Agriculture, Natural Resources Conservation Service (USDA NRCS). 2009. Web Soil Survey. http://Www.Websoilsurvey.Ncsc.Usda.Gov/App [Verified June 9, 2019].

US EPA. 1999. *Compendium of Methods for the Determination of Toxic Organic Compounds in Ambient Air*, (No. EPA/625/R-96/010a). Center for Environmental Research Information, National Risk Management Research Laboratory, Office of Research and Development. US Environmental Protection Agency (US EPA): Cincinnati, OH.

Velasco Ayuso S, Giraldo Silva A, Nelson C, Barger NN, Garcia-Pichel F. 2017. Microbial nursery production of high-quality biological soil crust biomass for restoration of degraded dryland soils. *Applied and Environmental Microbiology* **83**(3): 1–16. https://doi.org/10.1128/AEM.02179-16

Webb NP, Herrick JE, Van Zee JW, Courtright EM, Hugenholtz CH, Zobeck TM, Okin GS, Barchyn TE, Billings BJ, Boyd R, others. 2016. The National Wind Erosion Research Network: building a standardized long-term data resource for aeolian research, modeling and land management. *Aeolian Research* **22**: 23–36.

Williams J, Dobrowolski J, West N, Gillette D. 1995. Microphytic crust influence on wind erosion. *Transactions of the ASAE* **38**(1): 131–137.

Yang K, Tang Z. 2012. Effectiveness of fly ash and polyacrylamide as a sand-fixing agent for wind erosion control. *Water, Air, & Soil Pollution* **223**(7): 4065–4074.

Young TP, Petersen DA, Clary JJ. 2005. The ecology of restoration: historical links, emerging issues and unexplored realms. *Ecology Letters* **8**(6): 662–673. https://doi.org/10.1111/j.1461-0248.2005.00764.x

Zaady E, Katra I, Barkai D, Knoll Y, Sarig S. 2016. The coupling effects of using coal fly-ash and bio-inoculant for rehabilitation of disturbed biocrusts in active sand dunes. *Land Degradation & Development* **28**(4): 1228–1236. https://doi.org/10.1002/ldr.2510

Zang Y-X, Gong W, Xie H, Liu B-L, Chen H-L. 2015. Chemical sand stabilization: a review of material, mechanism, and problems. *Environmental Technology Reviews* **4**(1): 119–132.

Zhang B, Zhang Y, Su Y, Wang J, Zhang J. 2013. Responses of microalgal-microbial biomass and enzyme activities of biological soil crusts to moisture and inoculated *Microcoleus vaginatus* gradients. *Arid Land Research and Management* **27**(3): 216–230. https://doi.org/10.1080/15324982.2012.754514

Zhang Y, Wang H, Wang X, Yang W, Zhang D. 2006. The microstructure of microbiotic crust and its influence on wind erosion for a sandy soil surface in the Gurbantunggut Desert of northwestern China. *Geoderma* **132**: 441–449.

Supporting Information

Additional supporting information may be found online in the Supporting Information section at the end of the article.

Table S1 Irrigation records. Added volumes per plot and duration of wetness are approximate. Also reported in Fick et al., 2019, Supplemental Information.

Table S2 Measured variable averages by treatment. Standard errors in parentheses.

Table S3 Correlations between the index for estimating threshold friction velocity (TFV) cited in Li et al., 2010, and response variables in this study. P-value for Pearson correlation in parentheses. Equation used in Li et al was 4.095 + -.078 * [area of bb crater (cm2)] + 1.91 * [pocket penetrometer resistance (kg)]. Variables include instantaneous PM_{10} emissions in mg m^{-2} s^{-1} (flux), standard deviation in flux (fluxsd), accumulated PM_{10} emissions in µg at a given step (acc_p10), estimated threshold friction velocity (tfv), and emissions slope at each step (slope). The Ascending step includes all portions of the simulation where RPM is increasing, the decreasing step includes the end of the simulation, and the filter step includes readings where the ratio between target RPM and actual RPM is less than.95, for RPM steps between 0 and 5000.

Table S4 Correlation coefficients between measured parameters and PM10 flux at different PI-SWERL steps. P-value for Pearson correlation in parentheses

Figure S1 Identification of threshold friction velocity. Top panel depicts the cumulative PM_{10} curve, ignoring emissions at the constant steps in the PI-SWERL run. Bottom panel represents the local maximum of the second derivative, representing the threshold friction velocity.

Figure S2 Identification of DustTrak sensor 'spikes' likely related to dislodged saltating aggregates. For each 'step' in the PI-SWERL simulation (constant RPM), low frequency change was removed using a thin-plate spline. Peaks were identified as local maxima greater than 3 standard deviations greater than the mean. Standard deviations were obtained from detrended data. Readings at 0 RPM were excluded from analysis.

Figure S3 Differences in expected number of PM_{10} spikes (estimated marginal means) per simulation during constant RPM PI-SWERL 'steps' for plots inoculated ('TRUE') and not inoculated ('FALSE') with biocrust. Spikes were identified as peaks in the de-trended PM_{10} flux timeseries exceeding 3.5 standard deviations of the mean. Confidence bands represented by blue bars. The degree to which red arrows overlap reflects as much as possible the significance of the comparison of the pairwise estimates.

Figure S4 Distributions of hourly average and maximum windspeeds observed near study location compared to 20-year average for the period of February – May. Data comes from the 'Dugout Ranch' North Pasture USGS Clim-met station (SW04; Urban, 2017)